

Supporting information of

Metal–2D multilayered semiconductor junctions: Layer-number dependent Fermi-level pinning

Qian Wang,^{a,b} Yangfan Shao,^{a,c} Penglai Gong,^a and Xingqiang Shi^{a,*}

^a Department of Physics and Guangdong Provincial Key Laboratory for Computational Science and Material Design, Southern University of Science and Technology, Shenzhen 518055, China

^b Harbin Institute of Technology, Harbin 150080, China

^c Joint Key Laboratory of the Ministry of Education, Institute of Applied Physics and Materials Engineering, University of Macau, Macau, China

* E-mail: shixq@sustech.edu.cn

Contents:

- 1. Interface dipole in Pt-1L MoS₂ junction**
- 2. Structural relaxation in metal-MoS₂ junctions**
- 3. Projected band structures in metal-multilayered MoS₂ junctions**
- 4. *n*- to *p*-type contact transition**
- 5. Effect of metal strain on pinning factor *S***
- 6. Effect of metal surface roughness on pinning factor *S***
- 7. Effect of sulfur vacancy on Schottky barrier**

1. Interface dipole in Pt-1L MoS₂ junction

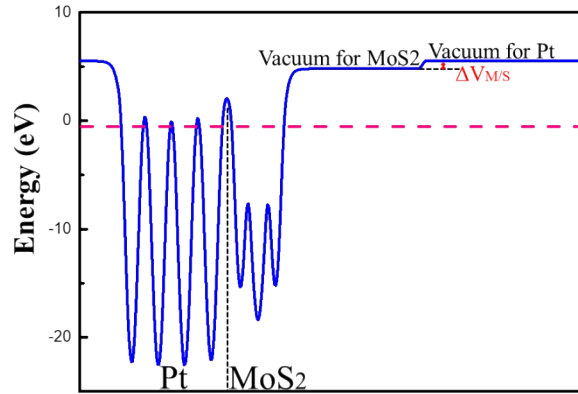


Fig. S1. Plane-averaged electrostatic potential along the interface normal direction in Pt-1L MoS₂ junction. The Fermi level is indicated by red dotted line. The interface potential step ΔV_{MS} is reflected in the energy difference between the work function on the metal side and on the MoS₂ side.

2. Structural relaxation in metal-MoS₂ junctions

The slab model of metal–MoS₂ junctions are composed of four layers of metal atoms and 1L to 7L of MoS₂. During structural relaxation, all atoms are free to relax except the outermost two metal layers are fixed to preserve its bulk property. The supercell and lattice mismatch between metal and MoS₂ are listed in Table SI. Details about the different atomic relaxations of the different systems are shown in Table SII.

Table SI. Supercell and lattice mismatch ($\sigma\%$) for metal/MoS₂ junctions [for example, “ $4 \times 4 / \sqrt{13} \times \sqrt{13}$ ” means MoS₂ with a ($\sqrt{13} \times \sqrt{13}$) cell adsorbed on Metal with a (4×4) cell]. Larger supercell results in smaller lattice mismatch, and vice versa.

Metal	Metal/MoS ₂	$\sigma\%$	Metal/MoS ₂	$\sigma\%$
Ag(111)	$4 \times 4 / \sqrt{13} \times \sqrt{13}$	1.44	$2 \times 2 / \sqrt{3} \times \sqrt{3}$	5.58
Cu(111)	$4 \times 4 / 5 \times 5$	0.77	$2 \times 2 / \sqrt{3} \times \sqrt{3}$	-6.92
Au(111)	$4 \times 4 / \sqrt{13} \times \sqrt{13}$	2.21	$2 \times 2 / \sqrt{3} \times \sqrt{3}$	6.37

Pd(111)	$2 \times 2/\sqrt{3} \times \sqrt{3}$	0.91	$2 \times 2/\sqrt{3} \times \sqrt{3}$	0.91
Pt(111)	$2 \times 2/\sqrt{3} \times \sqrt{3}$	1.85	$2 \times 2/\sqrt{3} \times \sqrt{3}$	1.85

The supercells for MoS₂ absorbed on different metal surfaces and their lattice mismatch are listed in Table SI. In making a reliable modeling, we change the metal lattice to fit the MoS₂ lattice, as did in this way in literature.¹⁻⁷ The lattice-mismatch ε is defined as $\sigma = (a - a_0)/a_0$, where a_0 and a are the in-plane supercell lattice of MoS₂ and metal surfaces, respectively. The two type supercells give same conclusion that pinning factor $S \approx 0.3$ (see Part V below), which is in consistent with previous theoretical results^{7,8} and indicates a strong pinning effect at metal-MoS₂ interface.

We then discuss the details of atomic relaxations in Metal-1L MoS₂, especially the fluctuations of interface atoms in the c-axis (the surface normal vacuum direction). The specific numbers of DHL_M, DHL_S, VAR_M, VAR_S, and D are shown in the following Table SII.

Table SII. The details of atomic relaxations in Metal-1L MoS₂. DHL_M and DHL_S mean the difference between the highest and lowest atomic coordinates in the c-direction of metal atoms and S atoms at interface, VAR_M and VAR_S represent the corresponding root square deviation, D represents the averaged equilibrium interface distance (vertical height difference) between surface metal atom and S atom of MoS₂.

Metal-MoS ₂	Metal atoms		S atoms		D (Å)
	DHL _M (Å)	VAR _M (Å)	DHL _S (Å)	VAR _S (Å)	
Ag-MoS ₂	0.074	5.26E-03	0.009	1.74E-04	2.85
Cu-MoS ₂	0.221	7.84E-03	0.110	4.77E-03	2.44
Au-MoS ₂	0.163	1.09E-02	0.020	7.88E-04	2.89
Pd-MoS ₂	0.042	8.39E-03	0.010	7.53E-04	2.34
Pt-MoS ₂	0.191	4.09E-02	0.034	8.65E-03	2.56

DHL represents the difference between the highest and lowest atomic coordinates in c-direction of atoms in an atomic plane, which means the maximum fluctuation of atoms in a plane, we defined it as:

$$\text{DHL} = H_C - L_C,$$

H_C and L_C mean the coordinates in c-direction of the highest and lowest atoms. VAR represents the root square deviation of the fluctuation, which means the average fluctuation of a plane:

$$\text{VAR} = \sqrt{\frac{\sum_{i=1}^n (C_i - C_{AVG})^2}{n}},$$

C means the c-coordinates of atoms in the same plane for the metal layer and the sulfur layer at interface, C_{AVG} means the average value of them. Over all, the atomic relaxations are small due to the van-der-Waals-like interaction between metal surface and MoS_2 .

3. Projected band structure in metal-multilayered MoS_2 junctions

Table SIII. SBHs for metal-1L MoS_2 , metal-2L MoS_2 , metal-3L MoS_2 , metal-7L MoS_2 junctions. Most of the numbers represent n -type SBH, while the numbers with superscript p represent p -type SBH.

	SBHs for metal-1L MoS_2 (eV)	SBHs for metal-2L MoS_2 (eV)	SBHs for metal-3L MoS_2 (eV)	SBHs for metal-7L MoS_2 (eV)
Ag(111)	0.14	0.12	0.13	0.14
Cu(111)	0.17	0.16	0.17	0.17
Au(111)	0.34	0.28	0.28	0.25
Pd(111)	0.60	0.58	0.33 ^p	0.32 ^p
Pt(111)	0.62	0.48 ^p	0.37 ^p	0.29 ^p

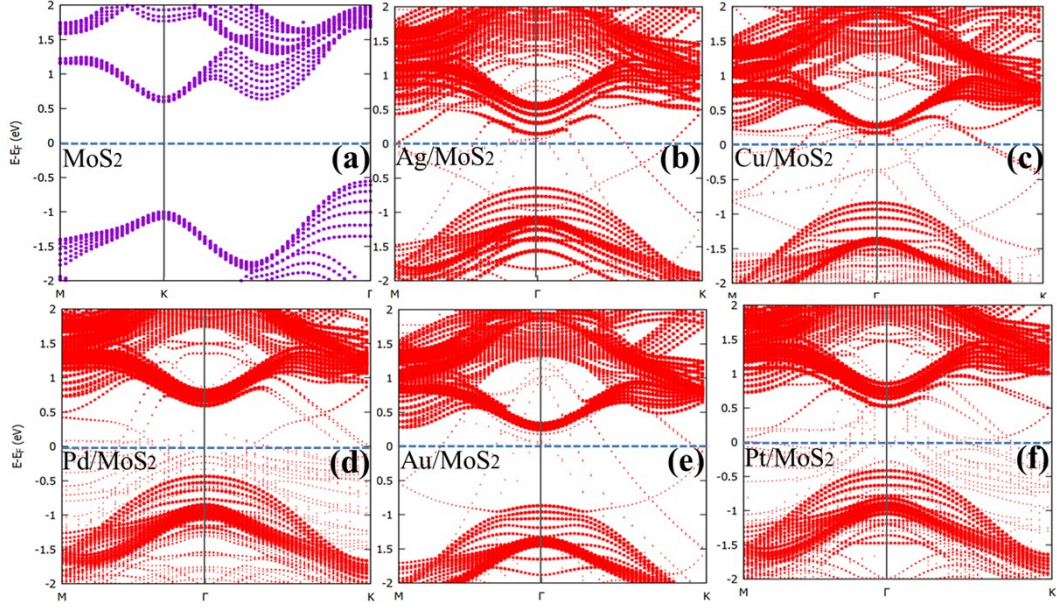


Fig. S2. (a) Band structure of 7L MoS₂, the unit cell is 1x1. (b-f), The projected band structures of MoS₂ in metal–7L MoS₂ heterojunctions, $\sqrt{3} \times \sqrt{3}$ MoS₂ cells were placed on top of 2×2 metal (111) surfaces for metal–MoS₂ junctions.

Metal–7L MoS₂ heterojunctions use $\sqrt{3} \times \sqrt{3}R30^\circ$ MoS₂ absorbed on 2×2 Ag (111), Au (111), Cu (111), Pd (111) and Pt (111) surfaces. As shown in the Table SII above, Ag–7L MoS₂, Cu–7L MoS₂, and Au–7L MoS₂ show electron Schottky barrier, the corresponding SBHs are 0.14 eV, 0.17 eV and 0.25 eV; Pd–7L MoS₂ and Pt–7L MoS₂ show hole Schottky barrier, the corresponding SBHs are 0.32 eV and 0.29 eV.

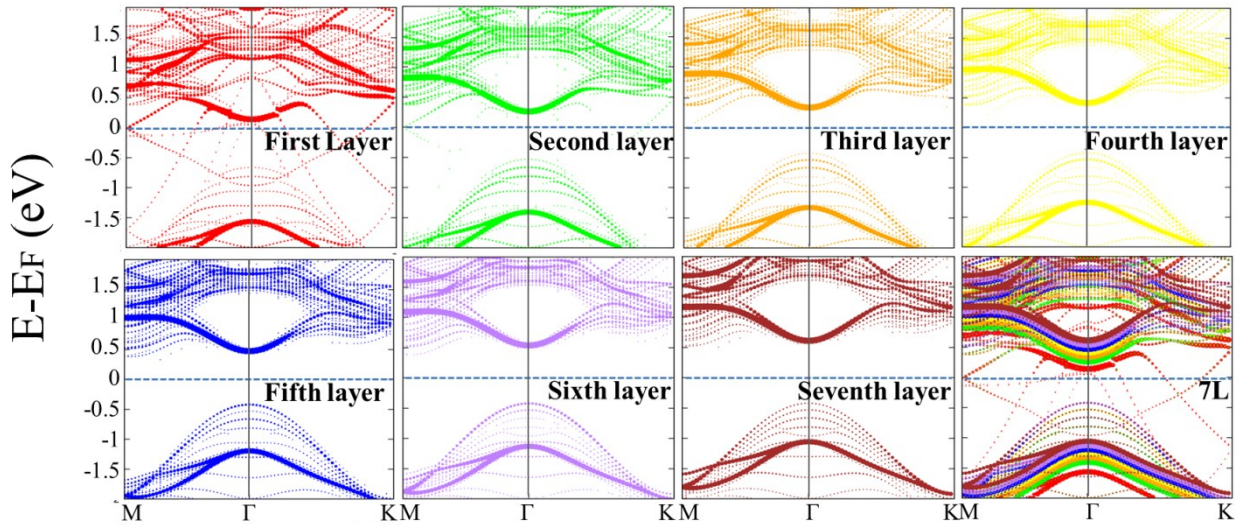


Fig. S3. Projected band structures of each layer in Ag–7L MoS₂. The Fermi level is set at $E = 0$ eV, shown by the

blue dotted line.

To discuss the depinning between MoS₂ layers, we plot the projected band structure for each MoS₂ layer in the 7L-MoS₂ junction in Fig. S3.

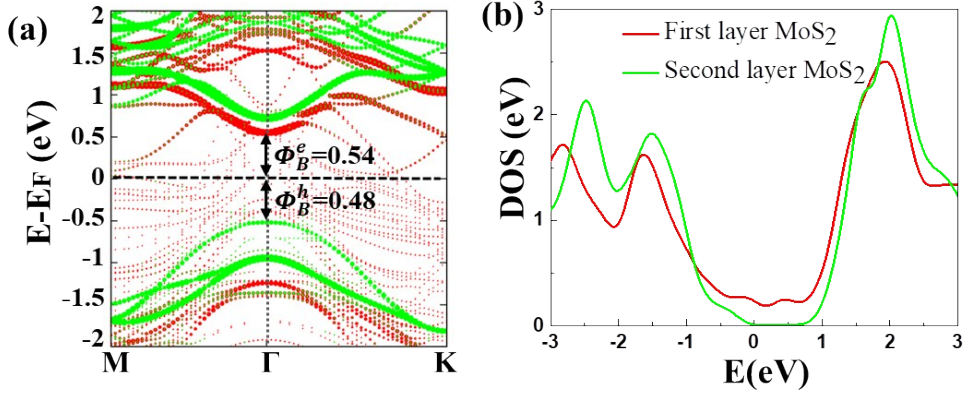


Fig. S4. (a) The projected band structure of the 2L MoS₂ in Pt-2L MoS₂ junctions. The contributions from the first and second layers are marked with red and green dot lines, respectively. The n-type SBH and p-type SBH are labeled with Φ_B^e and Φ_B^h . Fermi level was set to zero. (b) Partial DOS [with a Gaussian smearing of 0.05 eV] for the first and second layer of MoS₂ in junctions of Pt-2L MoS₂.

4. *N-* to *p-*type contact transition

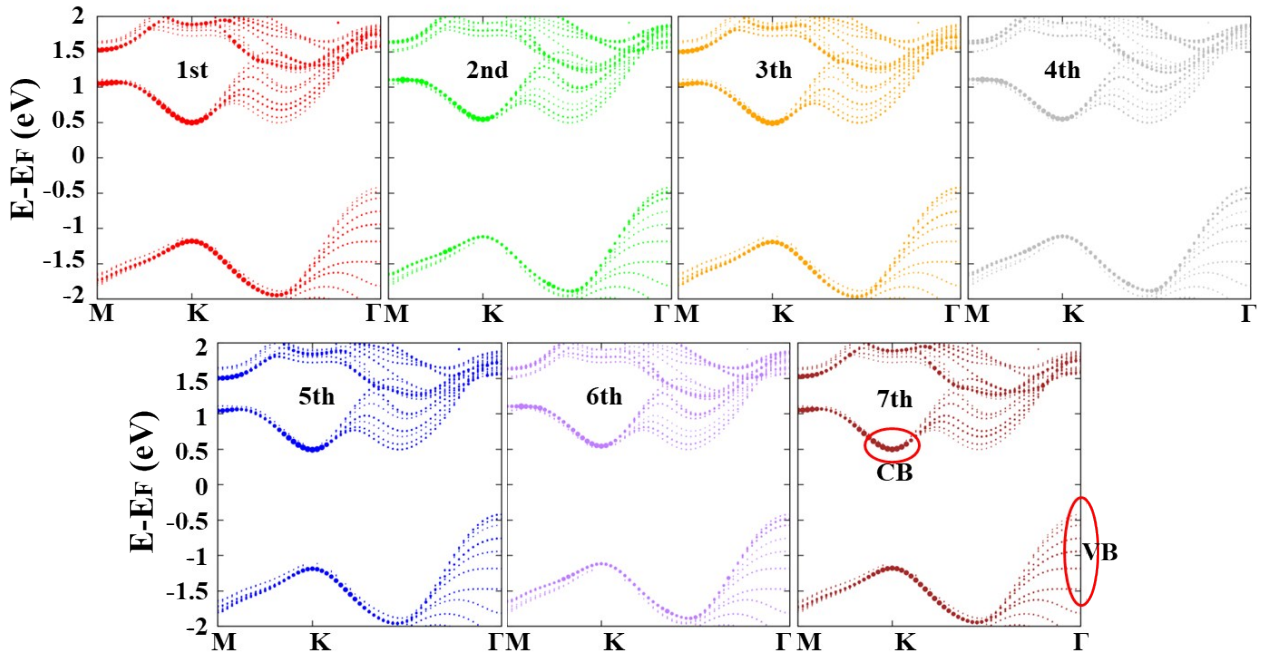


Fig. S5. Band structure projected to each layer of MoS₂ in isolated 7L MoS₂ without metal, the contributions from the 1st to 7th layers are shown with different colors. Note that the indirect band gap of CBM at *K* and VBM at Γ point, as labeled and denote by the ellipses in the right-bottom panel. The supercell is 1×1 .

It is well known that monolayer MoS₂ has a direct band gap at the high symmetry point *K* in the Brillouin zone. With increasing layer number to two or more layers, indirect band gap of CBM at *K* and VBM at Γ points is formed,⁹ as shown in Fig. S5 for the 7L case. The band structures of each layer of MoS₂ have the similar character, the sub-bands are degenerate for CB at *K* point while nondegenerate for VB at Γ point. Therefore, the depinning effect induced band offset of VB is not so obvious for multilayered MoS₂ contact to metal, because the VB at Γ is ‘broadened’ and blurred itself.

5. Effect of metal strain on pinning factor *S*

Table SIV. Different strain ($\epsilon\%$) of metal surface with different supercell sizes of metal/MoS₂ junctions [for example, “ $4 \times 4 / \sqrt{13} \times \sqrt{13}$ ” means MoS₂ with a ($\sqrt{13} \times \sqrt{13}$) cell adsorbed on Metal with a (4×4) cell]. Larger supercell results in smaller strain of metal, and vice versa.

Metal	Larger supercell of Metal / MoS ₂ junction	Smaller ϵ %	Smaller supercell of Metal / MoS ₂ junction	Larger ϵ %
Ag(111)	$4 \times 4 / \sqrt{13} \times \sqrt{13}$	1.44	$2 \times 2 / \sqrt{3} \times \sqrt{3}$	5.58
Cu(111)	$4 \times 4 / 5 \times 5$	0.77	$2 \times 2 / \sqrt{3} \times \sqrt{3}$	- 6.92
Au(111)	$4 \times 4 / \sqrt{13} \times \sqrt{13}$	2.21	$2 \times 2 / \sqrt{3} \times \sqrt{3}$	6.37
Pd(111)	$2 \times 2 / \sqrt{3} \times \sqrt{3}$	0.91	$2 \times 2 / \sqrt{3} \times \sqrt{3}$	0.91
Pt(111)	$2 \times 2 / \sqrt{3} \times \sqrt{3}$	1.85	$2 \times 2 / \sqrt{3} \times \sqrt{3}$	1.85

The different supercells for metal/MoS₂ junctions and the lattice strain of metal, $\epsilon\%$, are listed in Table SIV. Here, the lattice strain ϵ is defined as $\epsilon = (a_0 - a)/a_0$, where a_0 and a are the in-plane lattice constants of metal surface without and with strain, respectively. A positive number represents compressive strain of metal surface, and vice versa. Then we calculated two sets of SBHs for small

and large strains, and, both for Metal-1L MoS₂ and Metal-2LMoS₂ junctions, to check whether our main conclusion (that the increase of pinning factor S with increasing MoS₂ layer number) is robust to different strain. The calculated SBHs are listed in Table SV.

Table SV. Comparison of SBH (in eV) for metal-MoS₂ junctions with different strain in metal (using the supercells in Table RI). Most of the numbers represent n -type SBH, while the numbers with superscript p represent p -type SBH.

Metal	Smaller strain		Larger strain	
	Metal-1L MoS ₂	Metal-2L MoS ₂	Metal-1L MoS ₂	Metal-2L MoS ₂
Ag(111)	0.22	0.35	0.14	0.12
Cu(111)	0.49	0.46	0.17	0.16
Au(111)	0.45	0.47 ^{<i>p</i>}	0.34	0.28
Pd(111)	0.60	0.58	0.60	0.58
Pt(111)	0.62	0.48 ^{<i>p</i>}	0.62	0.48 ^{<i>p</i>}

$$S = \left| \frac{d\Phi_B}{d\Phi_M} \right|$$

We then fit these SBH values (using $S = \left| \frac{d\Phi_B}{d\Phi_M} \right|$) to get the Schottky pinning factors S . For junctions with larger strain, the fitted S are 0.39 and 0.62 for 1L and 2L MoS₂, respectively, which give an increasing of S with the increasing of MoS₂ layers; and, for junctions with smaller strain, the fitted S are 0.26 and 0.46 for 1L, and 2L MoS₂, respectively, which give the same conclusion (increasing of S with the increasing of MoS₂ layers). Hence, our main conclusion (the Schottky pinning factors S increase when layer number of MoS₂ goes from one to two) holds in junctions with both larger and smaller strain, which justified that our method is reliable for our main conclusion.

In summary, strain has effect on the SBH value for a certain junction, but the main conclusion of our work does not change, due to the layer-number dependent pinning factor is from *the depinning effect between MoS₂ layers* (which is irrelevant to metal strain).

6. Effect of metal surface roughness on pinning factor S

Table SVI. Comparison of SBH (in eV) for metal-MoS₂ junctions with ideal metal surfaces and the metal surfaces with one-fourth metal atom vacancy. Most of the numbers represent *n*-type SBH, while the numbers with superscript *p* represent *p*-type SBH.

Metal	Metal surface with vacancy		Ideal metal surface	
	Metal-1L MoS ₂	Metal-4L MoS ₂	Metal-1L MoS ₂	Metal-4L MoS ₂
Ag(111)	-0.06	0.06	0.14	0.13
Cu(111)	0.17	0.20	0.17	0.16
Au(111)	0.21	0.24	0.34	0.28
Pd(111)	0.51	0.45 ^{<i>p</i>}	0.60	0.30 ^{<i>p</i>}
Pt(111)	0.37	0.42 ^{<i>p</i>}	0.62	0.32 ^{<i>p</i>}

The SBH values of metal-MoS₂ junction with and without vacancy on metal surface are shown in Table SVI, and Schottky pinning factors *S* are then fitted in Fig. S6. For ideal surface without vacancy, the fitted *S* are 0.39 and 0.68 for 1L and 4L MoS₂, respectively, which give an increased *S* with the increasing MoS₂ layers; and, for junctions with vacancy, the fitted *S* are 0.34 and 0.61 for 1L and 4L MoS₂, respectively, which give the same conclusion (increasing of *S* with the increasing of MoS₂ layers). Furthermore, same conclusion is confirmed in metal-MoS₂ junctions with adatom on metal surface, *S* increased from 0.37 to 0.69 when the layer number of MoS₂ changed from 1 to 4. Therefore, our main conclusion (the Schottky pinning factors *S* increase when MoS₂ goes from monolayer to multilayer) holds in junctions both with and without defects on metal surface.

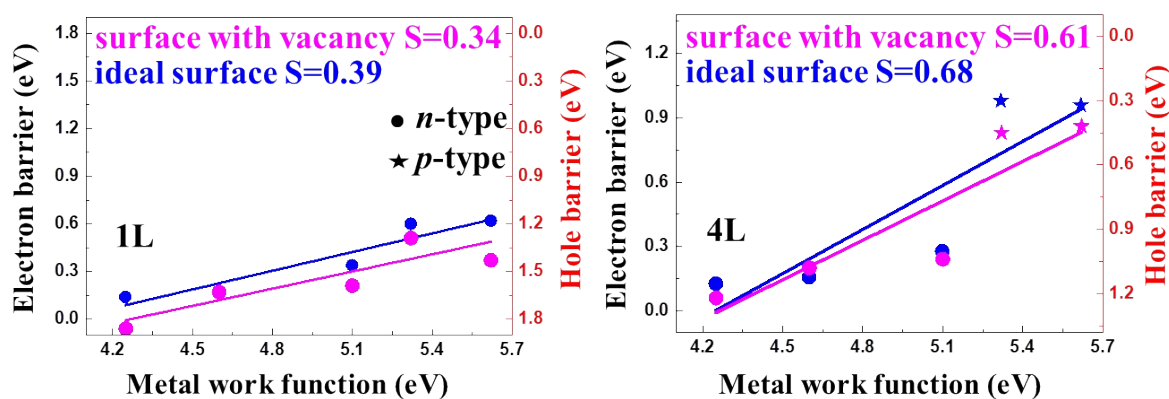


Fig. S6. Pinning factor S for 1L and 4L MoS₂. Pink and blue represent results of MoS₂ adsorbed on metal surface with vacancy and without vacancy, respectively. Dots and stars represent n-type and p-type Schottky barrier, respectively.

Actually, strain in metal surface and metal surface roughness has only a numerical effect on S , but does not affect its upward trend with increasing MoS₂ layer number. This can all be attributed to the physical nature that the layer-number dependent pinning factor S is from *the depinning effect between MoS₂ layers*. As we discussed in Fig. 3 in main text, in metal-multilayer MoS₂, strong pinning occurs only at the metal–first-layer MoS₂ interface and depinning occurs between MoS₂ layers. Metal can only intensively affect the first MoS₂ layer (or at most up to the third MoS₂ layer, the effect of the metal wave function on MoS₂ rapidly attenuates); therefore, metal surface strain and metal surface roughness can only change the numerical value of pinning factor S by affecting the pinning strength to the first MoS₂ layer, but has no direct relation to the screening effect between MoS₂ layers.

Also, we show the n-type (determined by the CBM of MoS₂ which is mainly contributed by the first layer) and p-type (determined by the VBM of MoS₂ which is mainly contributed by the other layers rather than the first layer) SBH varies with the number of layers in MoS₂-Pt junction with and without vacancy on Pt (111) surface in Fig. S7. As shown, the n-type SBH is almost unchanged, while the p-type SBH decreases with the increasing MoS₂ layers, which justified our conclusion (pinning occurs at the first MoS₂ layer while depinning occurs between MoS₂ vdW layers) is robust regardless of surface vacancy.

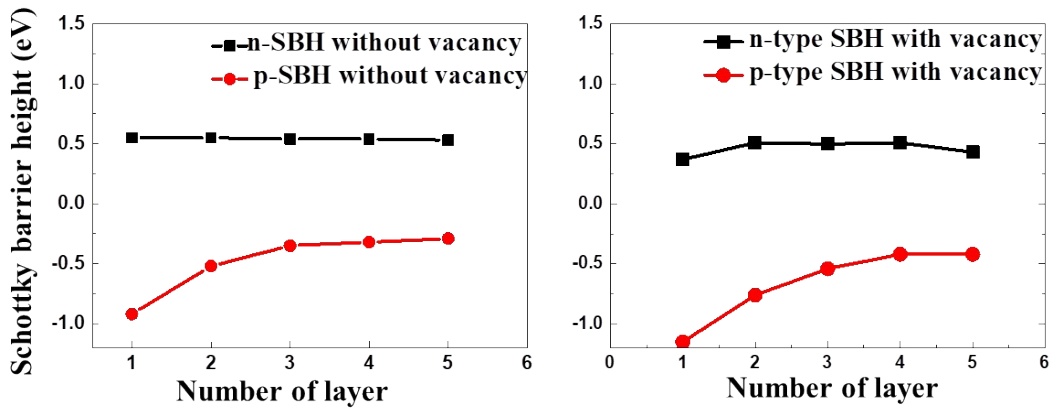


Fig. S7. SBH for MoS₂-Pt (without vacancy and with vacancy) junctions with 1L to 5L MoS₂.

In summary, metal surface strain and metal surface roughness have effect on the SBH value for a certain junction, but the main conclusion of our work does not change, due to the layer-number dependent pinning factor is from *the depinning effect between MoS₂ layers* (which is irrelevant to metal strain or surface roughness).

7. Effect of sulfur vacancy on Schottky barrier

It's known that, among all defect types of MoS₂, sulfur vacancy (SV) was found to have the lowest formation energy and frequently studied.¹⁰ The band structures of freestanding bilayer MoS₂ without and with defects were shown in Fig. S8a & 8b; it can be found that the defect states caused by SV appear in the band gap, and these defects states are localized at three Mo atoms close to the sulfur vacancy (Fig. S9). Two unoccupied deep levels which might act as compensation centers locate at about 0.4 eV below CBM and an occupied level tight on top of VBM.

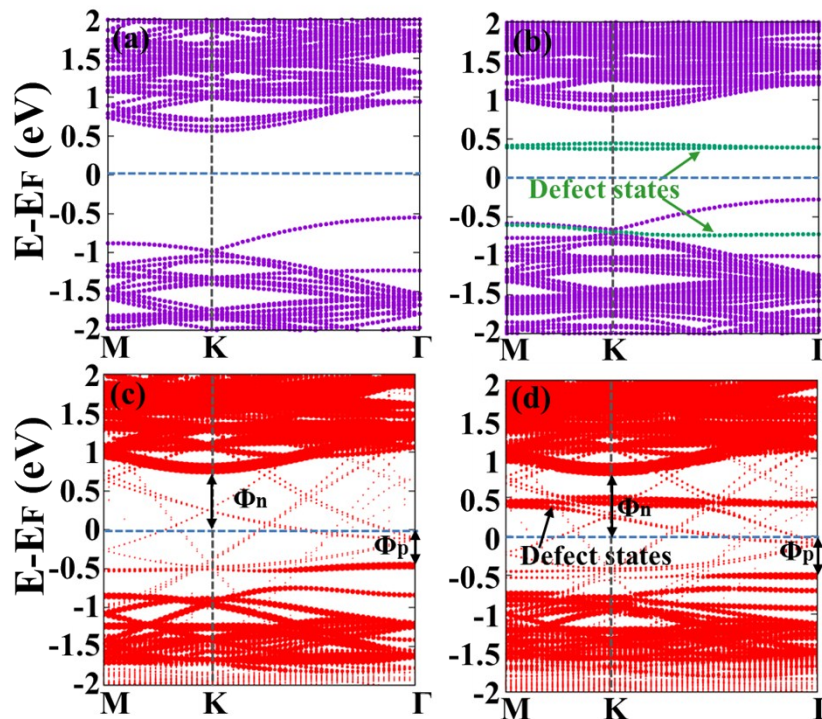


Fig. S8. Intrinsic sulfur vacancy in MoS₂ without and with substrates. Band structures of 2L freestanding MoS₂ (a) without defects, and (b) with 3.85% sulfur defect in one of MoS₂ layers. The Fermi-level is set at 0 eV, shown by blue dotted lines. Projected band structures of MoS₂ in Au-2L MoS₂ junctions (c) without defects, and (d) with a 3.85% sulfur defect at the MoS₂ layer contact to Au.

Sulfur defects at the interface contacting to metal electrodes in metal–MoS₂ heterojunction are energetically favorable than at other locations away from the metal surface. To consider the influence of SV on SBH in heterojunctions, we studied Au–2L MoS₂ junction with a 3.85% interface SV in the first MoS₂ layer, the band structure is shown in Fig. S8d. As comparison, band structure of Au–2L MoS₂ junction without defect is displayed in Fig. S8c. Similar to freestanding sulfur vacancy defective MoS₂, defect states generated by SV are located in the band gap of MoS₂. For, small lattice mismatch Au–2L MoS₂ junction without defect, the SBH appears as a p-type contact (Fig. S8c). As shown in Fig. S8d, for Au–2L MoS₂ junction with sulfur vacancy, electron and hole SBHs change a little with the introduction of mid-gap defect states, but the p-type contact still holds. Since, the SBHs are still decided by band edge of delocalized Bloch states rather than the localized defect states. However, the localized defect states will facilitate electron transport. Therefore, MoS₂ with vacancy defect gives a conclusion consistent with that of ideal MoS₂ on the contact type transformation in *MmSJ* for high work function metal.

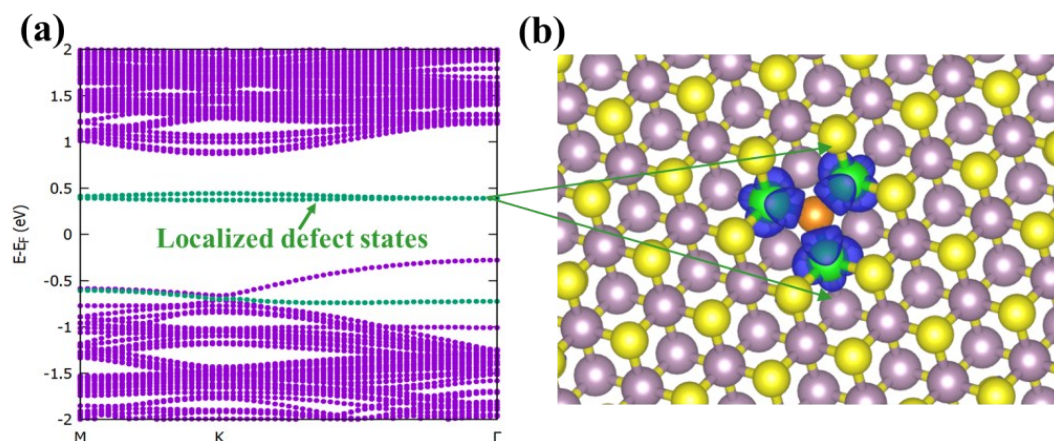


Fig. S9. (a) Band structures of 2L freestanding MoS₂ with 3.85% sulfur defect in one of MoS₂ layers. (b) Local charge densities of the defective MoS₂ at specific energy ranges. The energy range is 0 to 0.5 eV to include the defect states as indicated in Fig. (a). Blue bubbles indicate local charge densities. The position of sulfur vacancy is shown by orange sphere, and the three Mo atoms adjacent to the sulfur vacancy are marked with green spheres.

We analyze the local charge densities of defective MoS₂ at specific energy range of 0 to 0.5 eV of the band structure in Fig. S9a, and find the real-space distribution of defect states. Local charge densities are indicated by blue bubbles in Fig.S9b. As shown in Fig. S9b, the charge densities of defect states are localized on three Mo atoms adjacent to the sulfur vacancy.

References

- 1 M. Palsgaard, T. Gunst, T. Markussen, K.S. Thygesen, and M. Brandbyge, *Nano Lett.* **2018**, 18, 7275.
- 2 F. L. Ling, T W Zhou, X Q Liu, W Kang, W Zeng, Y X Zhang, L Fang, Y Lu and M Zhou, *Nanotechnology* **2018**, 29, 03LT01.
- 3 M. Farmanbar and G. Brocks, *Phys. Rev. B* **2016**, 93, 085304.
- 4 J. E. Padilha, A. Fazzio, and Antônio J. R. da Silva, *Phys. Rev. Lett.* **2015**, 114, 066803.
- 5 M. Farmanbar and G. Brocks, *Phys. Rev. B*, **2015**, 91, 161304.
- 6 Q. Wang, B. Deng, and X. Shi, *Phys. Chem. Chem. Phys.* **2017**, 19, 26151-26157.
- 7 C. Gong, L. Colombo, R. M. Wallace, K. Cho, *Nano Lett.* **2014**, 14, 1714-1720.
- 8 C. Kim, I. Moon, D. Lee, M. S. Choi, F. Ahmed, S. Nam, Y. Cho, H.-J. Shin, S. Park, W. J. Yoo, *ACS Nano* **2017**, 11, 1588-1596.
- 9 K. F. Mak, C. Lee, J. Hone, J. Shan, and T. F. Heinz, *Phys. Rev. Lett.* **2010**, 105, 136805.
- 10 W. Zhou et al., *Nano Lett.* **2013**, 13, 2615.